JACS
JOURNAL OF THE AMERICAN CHEMICAL SOCIETY
Article
pubs.acs.org/JACS

Selective Graphene Formation on Copper Twin Crystals

Kenjiro Hayashi,[†] Shintaro Sato,*[,†] Minoru Ikeda,[‡] Chioko Kaneta,[‡] and Naoki Yokoyama[†]

[†]Green Nanoelectronics Center (GNC), National Institute of Advanced Industrial Science and Technology (AIST), 16-1 Onogawa, Tsukuba, Ibaraki 305-8569, Japan

[‡]Next Generation Manufacturing Technologies Research Center, Fujitsu Laboratories Ltd, 10-1 Morinosato-Wakamiya, Atsugi, Kanagawa 243-0197, Japan

Supporting Information

ABSTRACT: Selective graphene growth on copper twin crystals by chemical vapor deposition has been achieved. Graphene ribbons can be formed only on narrow twin crystal regions with a (001) or high-index surface sandwiched between Cu crystals having (111) surfaces by tuning the growth conditions, especially by controlling the partial pressure of CH_4 in Ar/H_2 carrier gas. At a relatively low CH_4 pressure, graphene nucleation at steps on Cu (111) surfaces is suppressed, and graphene is preferentially nucleated and formed on twin crystal regions. Graphene ribbons as narrow as ~100 nm have been obtained in experiments. The preferential graphene nucleation and formation seem to be caused primarily by a difference in surface-dependent adsorption energies of reactants, which has been estimated by first principles calculations. Concentrations of reactants on a Cu surface have also been analyzed by solving a diffusion equation that qualitatively explains our experimental observations of the preferential graphene nucleation. Our findings may lead to self-organizing formation of graphene nanoribbons without reliance on top-down approaches in the future.

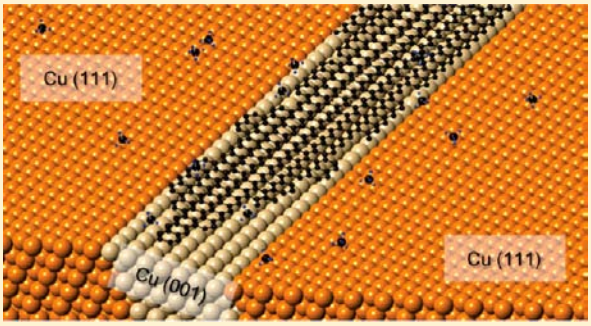

INTRODUCTION

Graphene, a two-dimensional carbon crystal, has excellent electrical properties originating from its peculiar band structure.[1,2] It is considered to be a promising electronic material owing to its extremely high carrier mobility and planar shape. For graphene to be used for electronics applications, it is desirable to prepare it on a large substrate in a controlled manner. In this context, graphene growth on polycrystalline metal foils and films by chemical vapor deposition (CVD) has been attempted recently,[3−6] while studies of graphene formation on a clean metal surface actually date back to the 1960s.[7−10] Graphene growth has been performed using metal catalysts, such as Ni,[3−5] Ru,[11,12] Ir,[13] and Fe,[6] but controlling the number of graphene layers using such catalysts is not easy. Li and co-workers found that single-layer graphene is predominantly formed on Cu foil.[14] Use of Cu as a catalyst enabled large-area single-layer graphene growth,[15,16] which is an important step toward real-world applications of graphene. Controlling graphene nucleation on a Cu surface would be the next step since it can affect the grain size of graphene,[17] which is an important parameter for electronics applications.

There have been several studies discussing graphene nucleation on a Cu surface.[17−25] Many of them argue that graphene nucleates at surface irregularities, such as grain boundaries,[20,24,25] surface steps,[22,23] surface particles,[20] and impurities.[20,22] However, at the same time, there are reports showing that graphene grows beyond surface steps and/or grain boundaries.[11,14,24] There should therefore be other factors that affect the nucleation. Here, we discuss how the Cu surface orientation affects graphene nucleation. In fact, the dependence of graphene growth on the orientation of Cu grains, which is not necessarily the same as the microscopic surface orientation, has recently been reported.[24,25] However, the growth rate and obtained products were mainly discussed. Moreover, these studies used Cu foils, which are known to have rough surfaces.[18,20] Therefore, for instance, grains with a nominal ⟨111⟩ orientation normal to the substrate may have surfaces with various orientations microscopically, which can actually affect nucleation. Therefore, it can be said that the dependence of the graphene nucleation on surface orientation is not yet well understood.

In this article, we demonstrate preferential graphene nucleation and growth on narrow Cu twin crystal regions that have a Cu (001) or high-index surface sandwiched between Cu crystals having (111) surfaces. The preferential graphene formation observed here suggests that graphene nucleation is affected by the surface orientation. We then show that the preferential nucleation can be explained by the difference in surface-dependent adsorption energies of reactants, which have been estimated by first principles calculations. Reactant concentrations on a Cu surface have also been analyzed by solving a diffusion equation, which qualitatively agrees with our experimental observations on the preferential graphene nucleation. Incidentally, we have succeeded in growing graphene ribbons as narrow as 100 nm and transferring them

Received: January 25, 2012
Published: July 10, 2012

   dx.doi.org/10.1021/ja300811p | J. Am. Chem. Soc. 2012, 134, 12492−12498

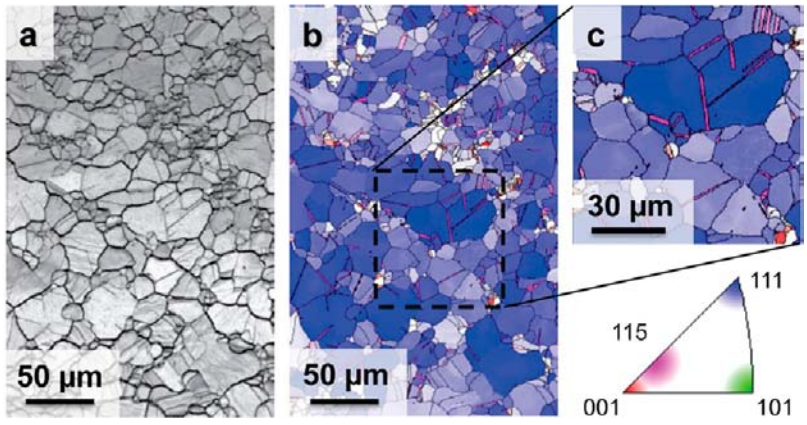

Figure 1. Cu film used for graphene growth. (a) SEM image of the Cu film after graphene growth. (b,c) Crystal orientation (normal to the substrate) maps of the Cu film after graphene growth obtained by EBSD along with an orientation index.

to a Si/SiO_2 substrate. Although these ribbons are still too wide to exhibit a large bandgap, our findings may lead to self-organizing graphene nanoribbon (GNR) formation through controlled graphene nucleation in the future.

RESULTS AND DISCUSSION

Graphene was grown at 860 °C on a $Cu/SiO_2/Si$ substrate by using CH_4 diluted by Ar and H_2 as the source gas (see Experimental Section for details). The thickness of the Cu film was 1000 nm. A scanning electron microscopy (SEM) image and crystal orientation map of the Cu film after graphene growth obtained by electron backscattered diffraction (EBSD) are shown in Figure 1. Most of the Cu grains are in the ⟨111⟩ direction normal to the substrate, as can be seen in Figure 1b. However, in the magnified image shown in Figure 1c, stripe-shaped regions with a ⟨115⟩ direction can be seen, which are Cu twin crystals.[26,27] We have found that graphene is formed preferentially on the surface of such Cu twin crystals. A SEM image of a Cu surface, which shows a Cu grain with several regions of twin crystals, is shown in Figure 2a. A cross sectional TEM image of such a region, shown in Figure 2b, indicates that graphene is actually formed on the twin crystal. The graphene formation has also been confirmed by Raman measurements on Cu, as shown in Figure 2c. An optical microscope image and Raman G-band map of a graphene ribbon transferred to a SiO_2/Si substrate are shown in Figure S1, Supporting Information. The twin crystal shown in Figure 2b has a high-index surface. On the other hand, the twin crystal region shown in Figure 2d has a Cu (001) surface on which graphene is formed. Observations of several twin crystals indicate that twin crystals have a (001) surface or a high-index surface. Such high-index surfaces are actually considered to consist of narrow (001) and (111) surfaces,[24] as illustrated in Figure 2e. Incidentally, it should be noted that the surface orientation of the twin crystal is different from the crystal orientation normal to the substrate, which is ⟨115⟩ in this case. The width of a graphene ribbon is controlled by that of the twin crystal region. While the graphene ribbons shown in Figure 2a have widths of several hundred nanometers, we have also obtained ones with widths of 100 nm or less, as shown in Figure 2f. Furthermore, by forming narrower twin crystals as demonstrated before,[28] it might be possible to grow GNRs with widths of 10 nm or less.

The dependence of graphene formation on the partial pressure of CH_4 is shown in Figure 3. The product of the partial pressure and the growth time were kept constant in all cases. When the partial pressure was low, graphene was formed only on the twin crystals. However, as the partial pressure was increased, graphene appeared to "spill out" from the twin crystal regions, as shown in Figure 3b. When the partial pressure was increased further, graphene nucleation began in areas other than the twin crystals, especially at steps on the Cu (111) surface. An interesting feature observed in Figure 3a is that graphene did not seem to nucleate at the boundaries of the twin crystal, which is different from some of the previous studies.[20,24,25] Particle-like defects as nucleation centers[20] were not observed either. Instead, nucleation seemed to occur anywhere on the surface of twin crystals. In fact, round-shaped graphene islands on the twin crystals can be seen in Figure 3a and Figure S2, Supporting Information. Such a shape strongly suggests that graphene does not nucleate from the boundaries. Our observation is in contrast with previous studies reporting graphene nucleation at surface irregularities, such as grain boundaries,[20,24,25] surface steps,[22,23] surface particles,[20] and impurities.[20,22] Incidentally, surface steps do work as nucleation centers at a relatively high partial pressure, as shown in Figure 3c. Our observation therefore means that the surface irregularities do work as nucleation centers under certain circumstances, although there is a recent report arguing that surface irregularities are not important for graphene nucleation.[18]

The observations described above suggest that preferential formation of graphene on twin crystals may arise from the existence of the Cu (001) surface. Namely, the nucleation of graphene islands may occur more easily on Cu (001) surfaces than on Cu (111) surfaces. There are recent studies discussing differences in graphene growth on Cu (111) and Cu (001) surfaces.[24,25,29] It was found that monolayer graphene was predominantly grown on a Cu (111) surface, while multilayer graphene was typically obtained on a Cu (001) surface.[24,25] Although these studies did not indicate the dependence of nucleation on surface orientation, the growth of multilayer graphene on a (001) surface may suggest easier nucleation on a (001) surface. However, this is not yet well understood.

As is well-known, nucleation is more likely to occur where the surface concentration of reactants is higher.[30] This situation can be achieved when the adsorption energy of reactants on the (001) surface is sufficiently higher than that on the (111) surface. At present, we are not sure what type of carbon species acts as the reactant for graphene nucleation. Therefore, we estimated adhesion energies of a carbon monomer (C), carbon

dx.doi.org/10.1021/ja300811p | J. Am. Chem. Soc. 2012, 134, 12492−12498

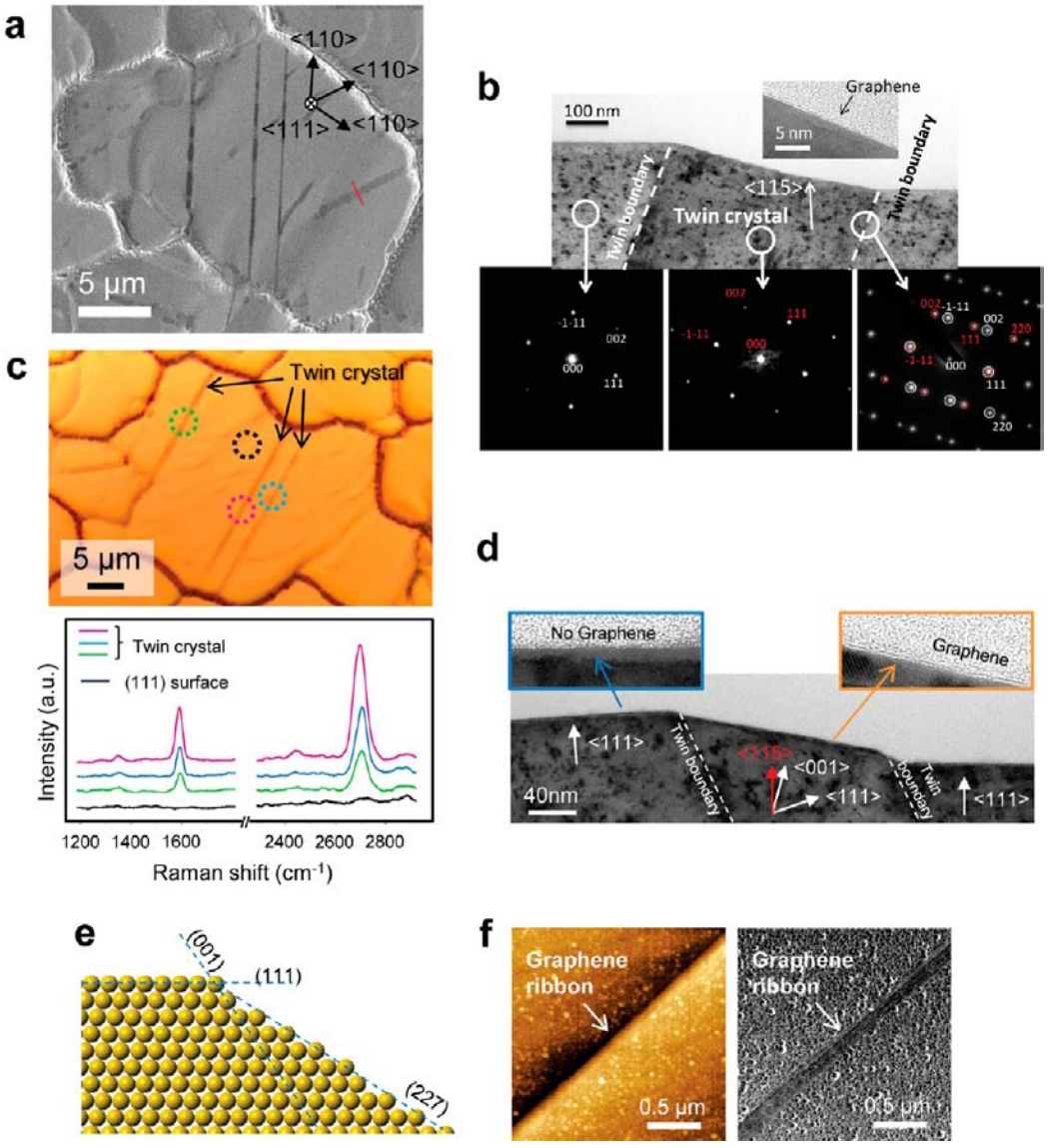

Figure 2. Graphene ribbons on Cu twin crystals. (a) SEM image of Cu grains with several twin crystal regions. The red line shows the position where the cross sectional TEM image shown in (b) was taken. (b) Cross sectional TEM images of the Cu film including a twin crystal along with electron diffraction patterns of the twin crystal and adjacent regions. Inset: Enlarged image of the surface of the twin crystal with graphene. (c) Optical microscope image of Cu grains including twin crystal regions on which graphene was grown. Raman spectra of the twin crystal and normal regions are also shown. (d) Cross sectional TEM images of a twin crystal region with a Cu (001) surface. Insets: Enlarged images of the Cu (111) surface and the twin crystal surface with graphene. (e) Schematic diagram of a high-index surface consisting of (001) and (111) surfaces. (f) Atomic force microscopy (tapping mode) images (left: topography image; right: phase image) of a graphene ribbon with a width of ~100 nm.

dimer (C_2), and acetylene molecule (C_2H_2) on Cu (111) and Cu (001) surfaces as possible nucleation reactants. For this purpose, we performed first principles calculations. The electronic states of the system were calculated by the projector augmented plane wave method (PAW_VASP) with generalized gradient approximation, GGA (PBE).[31−37] The details of the simulations are similar to those in a previous study,[38] and the Cu surface models used in the calculations are explained in the Supporting Information. In Figure 4a,d, we illustrate typical results for the adsorption energies of a monomer on the (111) and the (001) surfaces for several hollow, bridge, and top sites. A subsurface octahedral site, shown as S1 or S2 in Figure 4b, was also considered for the (111) surface; such sites are known to be the most stable sites for C monomers.[39,40] The most stable site on the (001) surface is the hollow site. The cases of C_2 and C_2H_2 were also investigated in a similar manner. The results are given in Table 1. Here, the adsorption energies were measured relative to that of a free monomer/dimer/C_2H_2. Figure 4b,e shows equilibrium positions of carbon monomers on (111) and (001) surfaces. The results clearly show that the adsorption energies on the (001) surface are larger in magnitude than those on the (111) surface for all the cases: The differences follow the order: monomer, C_2H_2, and dimer. Larger adsorption energies on the (001) surface for a carbon monomer and C_6 have also been obtained recently by Zhang et al.[41] Although we are not so sure what carbon species act as the reactant on the surfaces, it seems plausible to assume that many carbon species have a higher adsorption energy on the (001) surface than on the (111) surface.

We also calculated diffusion barriers of a carbon monomer, dimer, and C_2H_2 molecule on the Cu (111) and Cu (001) surfaces by using the nudged elastic band (NEB) method.[42] In

dx.doi.org/10.1021/ja300811p | J. Am. Chem. Soc. 2012, 134, 12492−12498

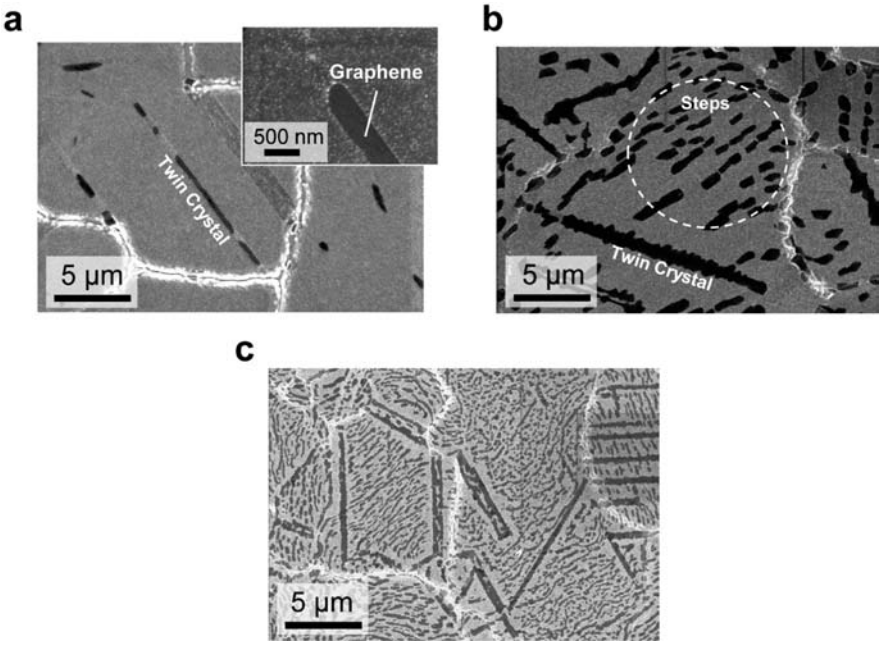

Figure 3. SEM images of Cu surfaces for dependence of graphene formation on the partial pressure of CH_4 (p_m) and growth time (t_g): (a) p_m = 0.091 Pa, t_g = 65 min; (b) p_m = 0.24 Pa, t_g = 25 min; and (c) p_m = 0.95 Pa, t_g = 10 min. The dark regions correspond to the regions where graphene was formed.

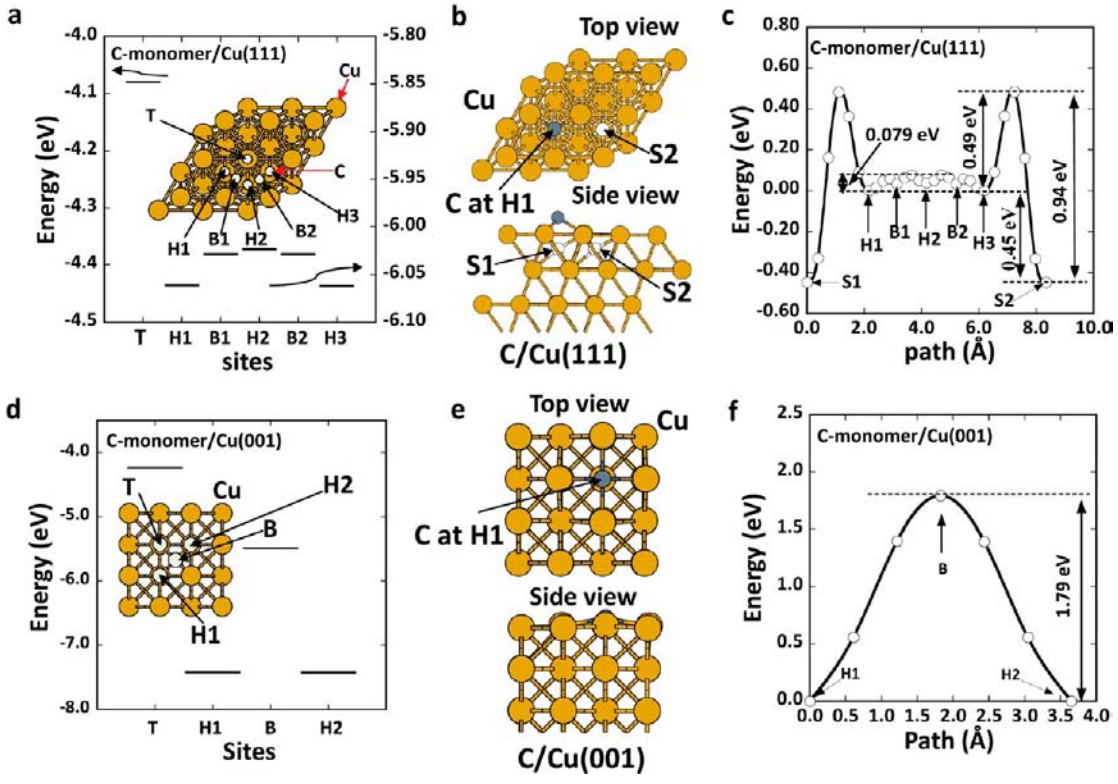

Figure 4. Adsorption energies for various monomer sites on the Cu (111) and Cu (001) surfaces. (a,d) Adsorption energies of a monomer for six different sites on the Cu (111) surface and for four sites on the Cu (001) surface, where the adsorption energy is measured relative to that of a free monomer. The inset illustrations show top views of the monomer adsorption sites, where H, B, and T indicate hollow, bridge, and top sites, respectively. (b,e) Top and side views of a monomer at H1 sites on the Cu (111) and Cu (001) surfaces. Two subsurface octahedral sites (S1 and S2) are also shown in the side view of Cu (111). (c,f) Energies along the NEB paths for a monomer on the Cu (111) and Cu (001) surfaces, where the energy at the H1 site was taken as the origin in each case. In the case of Cu (111) surface, the subsurface octahedral site S1 just below the H1 site is more stable than the H1 site at the top surface.

Figure 4c,f, we illustrate our typical NEB results for a monomer on Cu (111) and Cu (001) surfaces. The results including the cases for C_2 and C_2H_2 are given in Table 2. The diffusion barriers of a monomer, dimer, and C_2H_2 molecule are smaller

dx.doi.org/10.1021/ja300811p | J. Am. Chem. Soc. 2012, 134, 12492−12498

Table 1. Adsorption Energy (eV)

	carbon monomer	carbon dimer	C_2H_2
Cu (111)	−6.67	−5.84	−1.39
Cu (001)	−7.42	−5.93	−1.53

Table 2. Diffusion Barrier (eV)

	carbon monomer	carbon dimer	C_2H_2
Cu (111)	0.94	0.48	0.37
Cu (001)	1.79	0.86	0.76

on the (111) surface than on the (001) surface. Namely, these species diffuse more easily on the (111) surface than on the (001) surface. In fact, there is a study showing that graphene growth is fastest on the (111) surface,[24] which can be explained by the lower diffusion barrier on the (111) surface estimated here. Namely, once graphene has nucleated, it is natural to consider that it grows faster on a surface with a lower diffusion barrier. However, the implication of this result for the *nucleation process* is not very clear. Therefore, we investigated how the surface concentration of reactants, which could be any carbon species, is affected by the magnitudes of the adsorption energies and diffusion barriers, as described below.

In this model calculation, we assume the situation illustrated in Figure 5a. There is an elongated twin crystal region with a (001) surface sandwiched between Cu crystals with (111) surfaces. Since the length of the twin crystal region is much greater than its width, we can treat this as a one-dimensional problem. Here, we solve a one-dimensional diffusion equation to estimate the surface concentration of the reactants:[30]

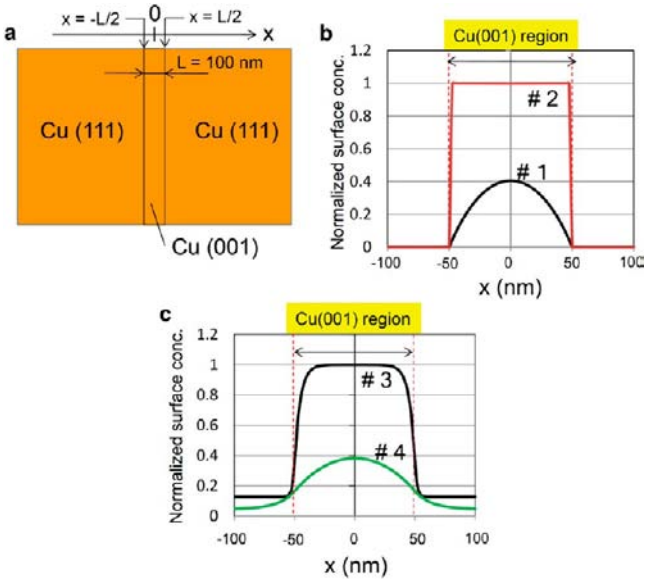

Figure 5. Surface concentration of reactants obtained by solving a diffusion equation. (a) Schematic diagram of the Cu surface used for the simulation. A narrow Cu (001) region is sandwiched between two Cu (111) regions. (b,c) Concentration profiles of the reactant molecules on the surface normalized by c_{001}: #1: $E_{diff,\ 001}$ = 0. 86, $E_{diff,\ 111}$ = 0.48 eV (E_{diff} values for carbon dimers were used), $E_{ads,\ 001}$ = −1.8, and $E_{ads,111}$ = −1.0 eV; #2: $E_{diff,\ 001}$ = 1.79, $E_{diff,\ 111}$ = 0.94 eV (E_{diff} values for carbon monomers were used), $E_{ads,\ 001}$ = −1.8, and $E_{ads,111}$ = −1.0 eV; #3: $E_{diff,\ 001}$ = $E_{diff,\ 111}$ = 0.5, $E_{ads,\ 001}$ = −1.0, and $E_{ads,111}$ = −0.8 eV; and #4: $E_{diff,\ 001}$ = $E_{diff,\ 111}$ = 0.5, $E_{ads,\ 001}$ = −1.5, and $E_{ads,111}$ = −1.2 eV.

$$D\frac{d^2c}{dx^2} - \frac{c}{\tau} + f = 0 \tag{1}$$

where c is the surface concentration of the reactants, D is the diffusion coefficient, τ is the lifetime of reactants on the surface, and f is the impingement rate of reactants onto the surface. The adsorption energy affects the surface concentration through τ (eq S3, Supporting Information), and the diffusion barrier, through D (eq S2, Supporting Information). Therefore, τ and D are different for surfaces with different indices. The impingement rate is assumed to be proportional to the partial pressure of the source gas (eq S4, Supporting Information). This equation can be solved analytically. Details are given in the Supporting Information. While the values for diffusion energy, E_{diff}, listed in Table 2 were used for the calculation, the values for adsorption energy, E_{ads}, in Table 1 were not used. Instead, E_{ads} was used as a parameter in this model calculation. This is because E_{ads} in Table 1, which was measured relative to the energy of each carbon species in vacuum, may not reflect the actual situation. In fact, it seems plausible that it should be measured relative to that of an intermediate species, as discussed in ref 41. Furthermore, carbon species like C_xH_y or CH_z could also be a reactant.[17,41] Therefore, we used only the qualitative result that E_{ads} on the (001) surface is higher than that on the (111) surface. The values of the other parameters are given in the Supporting Information.

Figure 5b,c shows the calculation results when the width of the (001) surface is 100 nm. The concentrations are normalized by the equilibrium concentration on the Cu (001) surface without diffusion, c_{001} (eq S9, Supporting Information). The two lines in Figure 5b are for different values of E_{diff}. One is the result using E_{diff} for the dimer (#1), and the other is for the monomer (#2). As for E_{ads}, we assumed that $E_{ads,111}$ and $E_{ads,\ 001}$ are −1.0 and −1.8 eV, respectively, which are about two times larger in magnitude than E_{diff} for the carbon dimer. It can be seen that the concentration profile is affected by E_{diff}. Curve #1 has a peak at the center of the (001) surface region and a parabolic shape, which may explain the situation shown in Figure 3a, where graphene islands with a circular shape can be seen. On the other hand, curve #2 is almost constant on the (001) surface, and it decreases rapidly near the boundary with the (111) surface. This situation is generally realized when the E_{ads} values are close to the E_{diff} values in magnitude, causing the diffusion length to decrease (see eq S8, Supporting Information). Incidentally, if the values listed in Table 1 are used for E_{ads}, the concentration becomes almost constant for the entire region, which is caused by large diffusion lengths resulting from the high E_{ads} values, suggesting no preferential formation on the (001) surface.

Here, we used different E_{diff} values from those listed in Table 2 in order to get a better understanding of the dependence on E_{diff}. Figure 5c shows the results for $E_{diff,\ 001}$ = $E_{diff,\ 111}$ = 0.5 eV. Curves #3 and #4 are for different E_{ads} values. In both cases, it can be seen that the concentration on the (111) surface is a little higher near the boundary, which is more likely to happen when E_{diff} values at the (111) and (001) surfaces are close to each other, and E_{ads} values are not very high in magnitude compared with E_{diff} values. This behavior might explain the situation shown in Figure 3b, where graphene sometimes spills out from the twin crystal region at a high source−gas pressure. Moreover, if the magnitude of E_{ads} is too high compared with that of E_{diff}, the concentration will be almost constant over the entire region, resulting in no preferential formation on the

dx.doi.org/10.1021/ja300811p | J. Am. Chem. Soc. 2012, 134, 12492−12498

(001) surface. One more notable finding is that preferential formation on an *isolated* narrower (001) surface occurs less easily, while graphene can be formed easily on an array of narrow (001) regions. This is probably why, at a high source–gas pressure, graphene starts to nucleate on surface steps, which probably have a very narrow (001) surface, as shown in Figure 3c. Our model calculation suggests that, in order to explain our experimental results, E_{diff} values at the (111) and (001) surfaces should be relatively close to each other and that E_{ads} values should be at most a few times higher in magnitude than those of E_{diff}.

In the model above, we did not take the dissociation of CH_4 on a Cu surface into consideration. The preferential formation may also be explained if the dissociation rate of CH_4 is higher on the (001) surface, which could be included in the diffusion model above. In fact, surface-dependent dissociation rates can be included in the diffusion equation as surface-dependent impingement rates, f, which affect equilibrium reactant concentrations on the (001) and (111) surfaces, as described in eqs S5 and S9, Supporting Information. In the situations shown in Figure 5b, where a possible difference in the dissociation rate is not considered, the equilibrium concentration on the (001) surface, c_{001}, is actually 3–4 orders of magnitude higher than that on the (111) surface, c_{111}. The considerable difference was caused by the difference in the adsorption energy. In this case, a minor difference in the dissociation rate would not affect the results. The difference in the dissociation rate would be important if the adsorption energies on the surfaces were close to each other. At this point, however, we do not have enough experimental and/or theoretical evidence for a difference in the dissociation rate, while there are a few past studies dealing with CH_4 dissociation on Cu.[43,44] This issue would therefore be a subject of future studies.

CONCLUSION

We have found that graphene ribbons can be formed preferentially on stripe-shaped surfaces of Cu twin crystals with a (001) or high-index surface sandwiched between Cu crystals having (111) surfaces. The preferential formation has been achieved primarily by controlling the partial pressure of CH_4 in Ar/H_2 carrier gas. The preferential nucleation and formation can be explained mainly by the difference in the adsorption energies of the reactants between the Cu (111) and Cu (001) surfaces. This kind of surface-dependent nucleation phenomenon on Cu was not well studied before and is in contrast with previous studies reporting graphene nucleation at surface irregularities, such as grain boundaries,[20,24,25] surface steps,[22,23] surface particles,[20] and impurities.[20,22] Our first principles calculations have actually shown that reactants have a higher adsorption energy on the (001) surface than on the (111) surface. Furthermore, concentrations of reactants on a Cu surface have been analyzed by solving a diffusion equation that qualitatively explains our experimental observations. Although the ribbon width obtained in the current study is still as narrow as ~100 nm, there is a possibility of forming narrower GNRs if we prepare a substrate with narrower twin crystal regions.[28]

EXPERIMENTAL SECTION

Graphene Growth. Graphene was grown on a Cu catalyst film deposited on a SiO_2/Si wafer by low-pressure thermal CVD.[6,14] The CVD system was a cold wall type with a heating stage on which the substrate was placed. The thickness of the Cu film, which was deposited by magnetron sputtering, was 1000 nm. The source gas was CH_4 diluted by Ar/H_2. The total gas pressure was kept at 1 kPa. The growth temperature was 860 °C, which was measured with a pyrometer. The substrate was first annealed for 20 min in Ar/H_2 mixture (flow rate: 1000/100 sccm), and CH_4 was then added for the growth. The growth time and the partial pressure of the CH_4 were changed to optimize the growth conditions.

Characterization. The synthesized graphene was characterized by SEM (Hitachi S-4800), TEM (Hitachi H-9000UHR III), Raman spectroscopy with an excitation wavelength of 488 nm (Horiba Jobin Yvon LabRAM HR-800), and atomic force microscopy (Shimadzu Nano Search Microscope SFT-3500). The EBSD analyses of the Cu film were performed using SEM (JEOL JSM-6500F) and orientation imaging microscope (TSL).

ASSOCIATED CONTENT

Supporting Information

Additional figures and description of modeling. This material is available free of charge via the Internet at http://pubs.acs.org.

AUTHOR INFORMATION

Corresponding Author

shintaro.sato@aist.go.jp

Notes

The authors declare no competing financial interest.

ACKNOWLEDGMENTS

This work was supported by JSPS through the FIRST Program, initiated by CSTP, Japan. This work was partly conducted at the Nano-Processing Facility supported by ICAN, AIST, Japan.

REFERENCES

(1) Novoselov, K. S.; Geim, A. K.; Morozov, S. V.; Jiang, D.; Zhang, Y.; Dubonos, S. V.; Grigorieva, I. V.; Firsov, A. A. *Science* **2004**, *306*, 666.
(2) Castro Neto, A. H.; Guinea, F.; Peres, N. M. R.; Novoselov, K. S.; Geim, A. K. *Rev. Mod. Phys.* **2009**, *81*, 109.
(3) Yu, Q.; Lian, J.; Siriponglert, S.; Li, H.; Chen, Y. P.; Pei, S.-S. *Appl. Phys. Lett.* **2008**, *93*, 113103.
(4) Reina, A.; Jia, X.; Ho, J.; Nezich, D.; Son, H.; Bulovic, V.; Dresselhaus, M. S.; Kong, J. *Nano Lett.* **2009**, *9*, 30.
(5) Kim, K. S.; Zhao, Y.; Jang, H.; Lee, S. Y.; Kim, J. M.; Ahn, J. H.; Kim, P.; Choi, J. Y.; Hong, B. H. *Nature* **2009**, *457*, 706.
(6) Kondo, D.; Sato, S.; Yagi, K.; Harada, N.; Sato, M.; Nihei, M.; Yokoyama, N. *Appl. Phys. Express* **2010**, *3*, 025102.
(7) May, J. W. *Surf. Sci.* **1969**, *17*, 267.
(8) Shelton, J. C.; Patil, H. R.; Blakely, J. M. *Surf. Sci.* **1974**, *43*, 493.
(9) Oshima, C.; Bannai, E.; Tanaka, T.; Kawai, S. *Jpn. J. Appl. Phys.* **1977**, *16*, 965.
(10) Hamilton, J. C.; Blakely, J. M. *Surf. Sci.* **1980**, *91*, 199.
(11) Sutter, P. W.; Flege, J. I.; Sutter, E. A. *Nat. Mater.* **2008**, *7*, 406.
(12) Pan, Y.; Zhang, H.; Shi, D.; Sun, J.; Du, S.; Liu, F.; Gao, H.-j. *Adv. Mater.* **2009**, *21*, 2777.
(13) Loginova, E.; Bartelt, N. C.; Feibelman, P. J.; McCarty, K. F. *New J. Phys.* **2008**, *10*, 093026.
(14) Li, X. S.; Cai, W. W.; An, J. H.; Kim, S.; Nah, J.; Yang, D. X.; Piner, R.; Velamakanni, A.; Jung, I.; Tutuc, E.; Banerjee, S. K.; Colombo, L.; Ruoff, R. S. *Science* **2009**, *324*, 1312.
(15) Li, X.; Zhu, Y.; Cai, W.; Borysiak, M.; Han, B.; Chen, D.; Piner, R. D.; Colombo, L.; Ruoff, R. S. *Nano Lett.* **2009**, *9*, 4359.
(16) Bae, S.; Kim, H.; Lee, Y.; Xu, X.; Park, J.-S.; Zheng, Y.; Balakrishnan, J.; Lei, T.; Kim, H. R.; Song, Y. I.; Kim, Y.-J.; Kim, K. S.; Ozyilmaz, B.; Ahn, J.-H.; Hong, B. H.; Iijima, S. *Nat. Nanotechnol.* **2010**, *5*, 574.

(17) Li, X.; Magnuson, C. W.; Venugopal, A.; An, J.; Suk, J. W.; Han, B.; Borysiak, M.; Cai, W.; Velamakanni, A.; Zhu, Y.; Fu, L.; Vogel, E. M.; Voelkl, E.; Colombo, L.; Ruoff, R. S. *Nano Lett.* **2010**, *10*, 4328.
(18) Luo, Z.; Lu, Y.; Singer, D. W.; Berck, M. E.; Somers, L. A.; Goldsmith, B. R.; Johnson, A. T. C. *Chem. Mater.* **2011**, *23*, 1441.
(19) Chen, H.; Zhu, W.; Zhang, Z. *Phys. Rev. Lett.* **2010**, *104*, 186101.
(20) Han, G. H.; Gunes, F.; Bae, J. J.; Kim, E. S.; Chae, S. J.; Shin, H. J.; Choi, J. Y.; Pribat, D.; Lee, Y. H. *Nano Lett.* **2011**, *11*, 4144.
(21) Yu, Q.; Jauregui, L. A.; Wu, W.; Colby, R.; Tian, J.; Su, Z.; Cao, H.; Liu, Z.; Pandey, D.; Wei, D.; Chung, T. F.; Peng, P.; Guisinger, N. P.; Stach, E. A.; Bao, J.; Pei, S.-S.; Chen, Y. P. *Nat. Mater.* **2011**, *10*, 443.
(22) Nie, S.; Wofford, J.; Bartelt, N.; Dubon, O.; McCarty, K. *Phys. Rev. B* **2011**, *84*, 155425.
(23) Wofford, J. M.; Nie, S.; McCarty, K. F.; Bartelt, N. C.; Dubon, O. D. *Nano Lett.* **2010**, *10*, 4890.
(24) Wood, J. D.; Schmucker, S. W.; Lyons, A. S.; Pop, E.; Lyding, J. W. *Nano Lett* **2011**, *11*, 4547.
(25) Ishihara, M.; Koga, Y.; Kim, J.; Tsugawa, K.; Hasegawa, M. *Mater. Lett.* **2011**, *65*, 2864.
(26) Pande, C. S.; Imam, M. A.; Rath, B. B. *Metal. Trans. A* **1990**, *21*, 2891.
(27) Mahajan, S.; Pande, C. S.; Imam, M. A.; Rath, B. B. *Acta Mater.* **1997**, *45*, 2633.
(28) Lu, L.; Shen, Y. F.; Chen, X. H.; Qian, L. H.; Lu, K. *Science* **2004**, *304*, 422.
(29) Zhao, L.; Rim, K. T.; Zhou, H.; He, R.; Heinz, T. F.; Pinczuk, A.; Flynn, G. W.; Pasupathy, A. N. *Solid State Commun.* **2011**, *151*, 509.
(30) Markov, I. V. *Crystal Growth for Beginners, Fundamentals of Nucleation, Crystal Growth and Epitaxy*; World Scientific: Singapore, 1995.
(31) Blöchl, P. E. *Phys. Rev. B* **1994**, *50*, 17953.
(32) Vanderbilt, D. *Phys. Rev. B* **1990**, *41*, 7892.
(33) Kresse, G.; Hafner, J. *Phys. Rev. B* **1993**, *47*, 558.
(34) Kresse, G.; Furthmuller, J. *Comput. Mater. Sci.* **1996**, *6*, 15.
(35) Kresse, G.; Furthmuller, J. *Phys. Rev. B* **1996**, *54*, 11169.
(36) Kresse, G.; Joubert, D. *Phys. Rev. B* **1999**, *59*, 1758.
(37) Perdew, J. P. *Phys. Rev. Lett.* **1985**, *55*, 1665.
(38) Ikeda, M.; Yamasaki, T.; Kaneta, C. *J. Phys.: Condens. Matter* **2010**, *22*, 384214.
(39) Yazyev, O. V.; Pasquarello, A. *Phys. Rev. Lett.* **2008**, *100*, 156102.
(40) Riikonen, S.; Krasheninnikov, A. V.; Halonen, L.; Nieminen, R. M. *J. Phys. Chem. C* **2012**, *116*, 5802.
(41) Zhang, W. H.; Wu, P.; Li, Z. Y.; Yang, J. L. *J. Phys. Chem. C* **2011**, *115*, 17782.
(42) Henkelman, G.; Jonsson, H. *J. Chem. Phys.* **2000**, *113*, 9978. In this article, we used the NEB VTST code combined with the PAW-VASP code. The VTST codes are the transition-state search codes provided by Prof. G. Henkelman's group, University of Texas, see: http://theory.cm.utexas.edu/vtsttools/.
(43) Alstrup, I.; Chorkendorff, I.; Ullmann, S. *Surf. Sci.* **1992**, *264*, 95.
(44) Lin, Y. Z.; Sun, J.; Yi, J.; Lin, J. D.; Chen, H. B.; Liao, D. W. J. *Mol. Struct.* **2002**, *587*, 63.